# Theoretical Study of the Oxidation Mechanisms of Naphthalene Initiated by Hydroxyl Radicals. II. The H Abstraction Pathway

Abolfazl Shiroudi and Michael S. Deleuze
Center of Molecular and Materials Modelling, Hasselt University,
Agoralaan, Gebouw D, B-3590 Diepenbeek, Belgium

## 1. INTRODUCTION

The gas-phase reaction between hydroxyl radicals and naphthalene has been experimentally studied at $T < 410$ K and at temperatures ranging from 636 to 873 K, by means of laser flash photolysis using laser-induced fluorescence, at pressures comprised between 6 and 128 mbar, under inert (He) conditions. At $T \leq 410$ K and $T \geq 600$ K, a least-squares analysis of the temperature dependence of the measured rate constants yields the following Arrhenius expressions:

$$k_{(T\leq 410K)} = \left(1.05^{+1.11}_{-0.54}\right)\times 10^{-12} e^{(902\pm 240)/T} \quad \text{cm}^3 \text{ molecule}^{-1} \text{ s}^{-1}$$

$$k_{(T\geq 600K)} = \left(1.12^{+2.12}_{-0.73}\right)\times 10^{-17} T^2 e^{-(969\pm 752)/T} \quad \text{cm}^3 \text{ molecule}^{-1} \text{ s}^{-1}$$

where the indicated errors correspond to two least-squares standard deviations. The first regression implies a negative activation energy, which can be interpreted as to correspond to the addition of OH radicals and its equilibration. In contrast, the second regression implies a positive activation energy, which has been ascribed to hydrogen abstraction. Great care is required in using DFT energy barriers, because these data are known in general to be strongly dependent on the employed exchange-correlation functional.

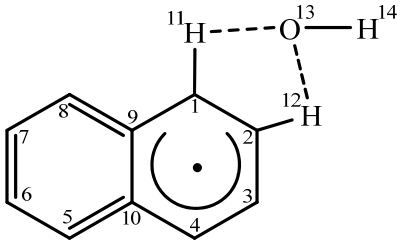


**Figure 1.** Retained atom labeling for characterizing the structures of intermediate and transition states

Besides providing energy barriers and reaction energies at a many-body quantum mechanical level of theory (CBS-QB3), the purposes of the present work is to supply kinetic equations, kinetic rate constants and branching ratios for the purpose of fully unraveling the original experiments on hydrogen abstraction from naphthalene by hydroxyl radicals at high temperatures ($T \geq 600$ K). See Figure 2 for the correspondingly investigated reaction pathways, **1** and **2**, leading to the 1-naphthyl (P1) and 2-naphthyl (P2) radicals, respectively.

## 2. COMPUTATIONAL DETAILS

The CBS-QB3 method was developed with the idea that a major source of error in quantum mechanical calculations arises from truncation of the basis set. The $N^{-1}$ asymptotic convergence of MP2 pair energies calculated from pair natural orbital expansions is used to extrapolate energies to the limit of a complete basis set (CBS). Kinetic parameters for the reaction pathways depicted in Figure 2 were correspondingly calculated by means of transition state theory (TST). Thermodynamic state functions were obtained from canonical partition functions that were computed for an ideal gas, using Boltzmann statistical thermodynamics along with the Rigid Rotor-Harmonic Oscillator approximation (RRHO).

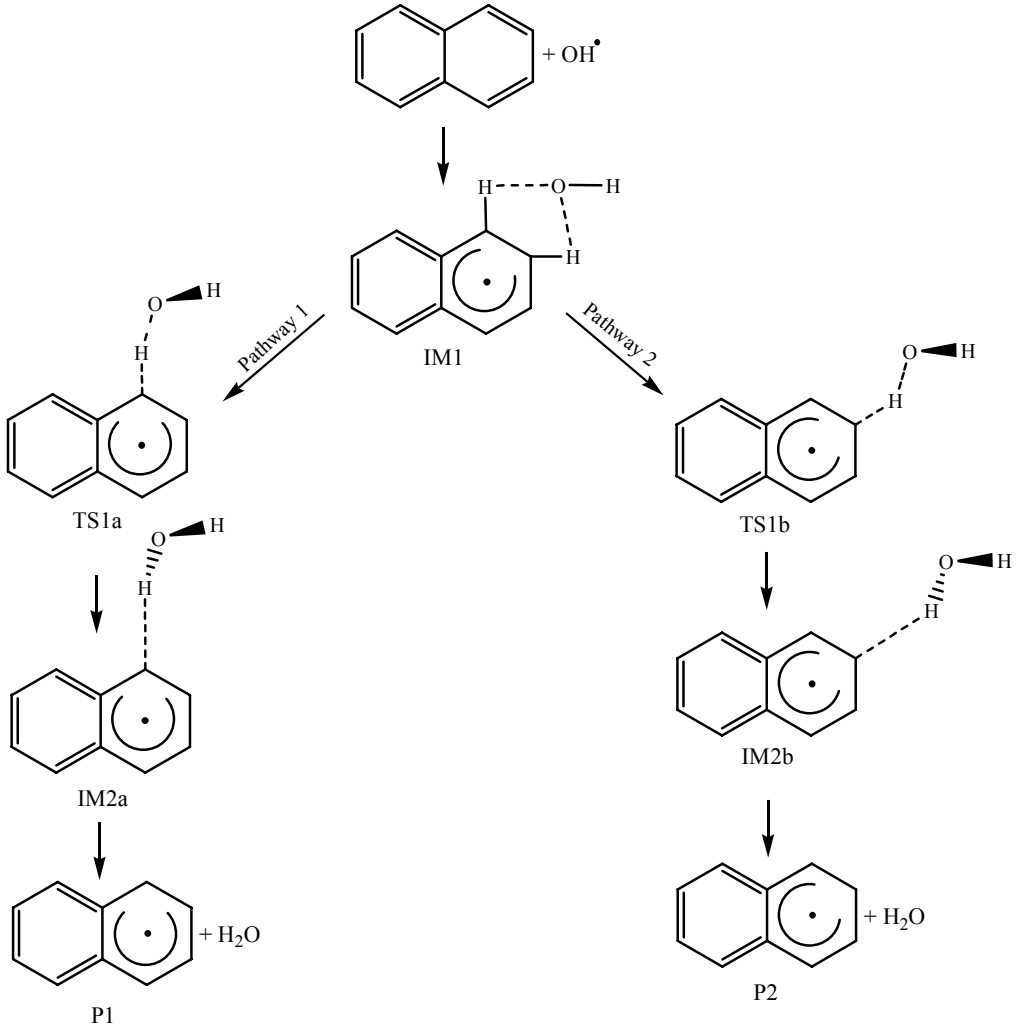


**Figure 2.** Reaction pathways for H-abstraction at the $C_1$ and $C_2$ positions in naphthalene by hydroxyl radicals, yielding water and 1-naphtyl (P1) or 2-naphthyl (P2) radicals.

The CBS approach is known to yield a mean absolute deviation of 1.1 kcal $mol^{-1}$ on the G2/97 test set for reaction energies. A more recent work indicates a maximum error of 2.8 kcal $mol^{-1}$ for the G2 test set of reaction energies, as well as average and mean absolute errors of 0.2 and 0.98 kcal $mol^{-1}$. This is only in case of an extreme spin contamination of the underlying UHF wave functions that more accurate but also much more costly methods, such as the G2 or G4 approaches, should be used. However, spin-contamination for doublet

radicals is known to be very small in symmetry-broken UHF-based CCSD calculations, even when the UHF spin contamination is very large. For example, for the $NO_2$ radical, for UHF and UHF-based CCSD wave functions, the value of $\langle S^2 \rangle$ is 1.18 and 0.76, respectively.

In our study, the removal of hydrogen atoms from naphthalene by OH radicals is analyzed according to a two-step reaction scheme, involving first a fast pre-equilibrium between the reactants ($C_{10}H_8$ and OH radicals) and a pre-reactive complex (IM1), followed by the abstraction of a hydrogen atom leading to a post-reactive complex (IM2) and, then to the products (1-naphthyl [P1] and 2-naphtyl [P2] radicals):

$$\text{step 1 : } C_{10}H_8 + OH^{\bullet} \underset{k_{-1}}{\overset{k_1}{\rightleftharpoons}} C_{10}H_8 \cdots OH^{\bullet}$$

$$\text{step 2 : } C_{10}H_8 \cdots OH^{\bullet} \xrightarrow{k_2} C_{10}H_7^{\bullet} + H_2O$$

A steady-state analysis of the overall reaction pathway leads to the following expression for the associated rate constant:

$$k_{\text{overall}} = \frac{k_1 k_2}{k_{-1} + k_2} \tag{1}$$

Even though the energy barrier for $k_{-1}$ has about the same height as that for $k_2$, the entropy change for the reverse reaction (IM1→R) is much larger than that for the formation of the products (IM1→P). Thus, $k_{-1}$ is expected to be considerably larger than $k_2$. Therefore, the overall rate constant can be rewritten as:

$$k_{overall} = K_c \, k_2 \tag{2}$$

with $K_c = k_1/k_{-1}$ the equilibrium constant for fast pre-equilibrium between the reactants and the pre-reactive complex (step 1):

$$K_c = \frac{\left[ C_{10}H_8 ... OH^{\bullet} \right]}{\left[ C_{10}H_8 \right] \left[ OH^{\bullet} \right]} \tag{3}$$

Using statistical thermodynamics, this equilibrium constant can be obtained according to:

$$K_c = \frac{Q_{\text{IM1}}}{Q_{\text{naph}} . Q_{OH^{\bullet}}} \times \frac{V_m(T)}{N_{\text{Av}}} \times \exp\left[ -\frac{\left( E_{\text{IM1}} - E_{\text{naph}} - E_{OH^{\bullet}} \right)}{RT} \right] \tag{4}$$

with $V_m(T) = RT/P$ the molar volume of an ideal gas. The kinetic rate constant characterizing the unimolecular dissociation reaction of the pre-reactive complex is obtained in the high pressure limit by means of transition state theory (TST):

$$k_2 = \kappa(T) \times \frac{\sigma k_B T}{h} \times \frac{Q_{\text{TS1}}}{Q_{\text{IM1}}} \times \exp\left[ -\frac{\left( E_{\text{TS1}} - E_{\text{IM1}} \right)}{RT} \right] \tag{5}$$

In eq. (5), $\kappa(T)$ and $\sigma$ denote the tunneling factor and reaction symmetry number characterizing step 2:

$$\kappa(T) = 1 + \frac{1}{24}\left(\frac{h\nu_i}{k_B T}\right)^2 \quad (6)$$

where $\nu_i$ is the imaginary vibrational frequency characterizing the transition state. Therefore, upon combining eqs. (3-5), we find:

$$k_{\text{overall}} = \frac{\sigma k_B T}{h} \times \frac{Q_{\text{TS1}}}{Q_{\text{naph}} . Q_{\text{OH}^\bullet}} \times \frac{V_m(T)}{N_{\text{Av}}} \times \exp\left(-\frac{\Delta E_o}{RT}\right) \quad (7)$$

with $\Delta E_o$ the net vibrationally adiabatic barrier for the overall reactions scheme:

$$\Delta E_o = E_{\text{TS1}} - E_{\text{Naph}} - E_{\text{OH}^\bullet} \quad (8)$$

Thus, the vibrationally adiabatic barrier at high pressures can be calculated as the difference between the energies of the transition states and reactants, without having at first glance to consider the pre-reactive complex. Because of quantum mechanical tunneling through the IM1→TS1x→IM2x (x=a,b) energy barriers, reactant complexes in addition channels are nevertheless essential for quantitative calculations of hydrogen abstraction rate constants.

## 3. RESULTS AND DISCUSSION

### *3.1. Structural characteristics of stationary points*

A pre-reactive molecular complex (IM1) has been identified (Figure 2) in the reactions of naphthalene with OH radicals, which finds its origin into long-range coulomb interactions between the reactant molecules. According to the CBS-QB3 data, this intermediate complex is located at about 2.5 kcal mol$^{-1}$ below the total energy of the reactants. Proceeding further along reaction pathways **1** or **2**, the abstraction process of $H_{11}$ or $H_{12}$ via the transition states TS1a and TS1b require activation energies of ~2.2 and ~2.4 kcal mol$^{-1}$ relative to the reactant energies (Figure 3).

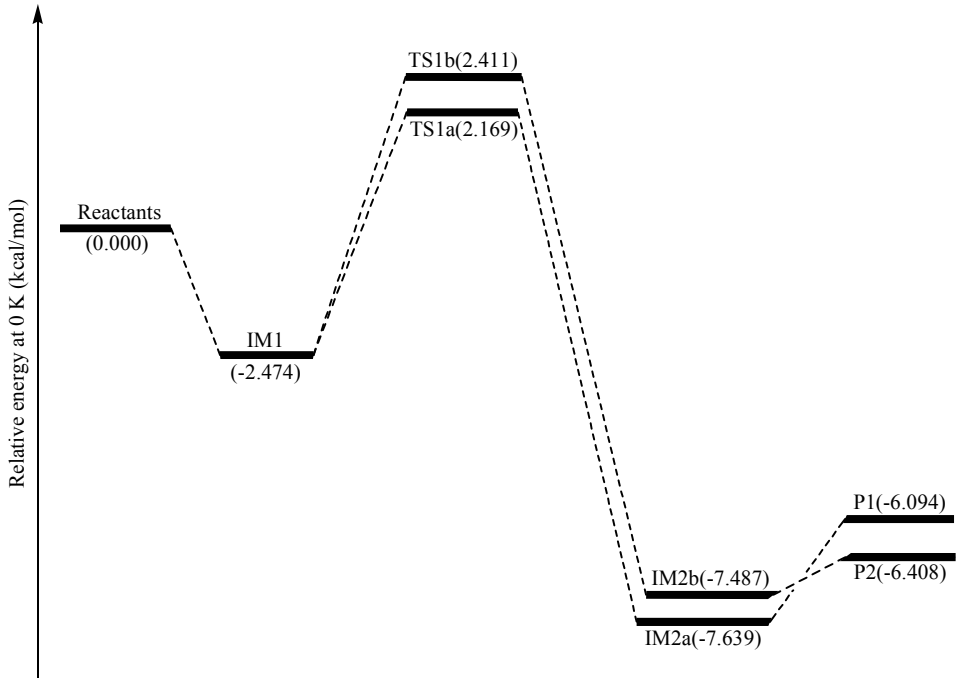


**Figure 3.** Potential energy diagram for the reaction pathways **1–2** obtained using the CBS-QB3 method

Two post-reactive molecular complexes IM2a and IM2b are identified further on the product side of the reaction barriers, which corresponds to the dissociation of IM1 into a water molecule and a 1- or 2-naphthyl radical species. These post-reactive molecular complexes are stabilized by a hydrogen bonding between the oxygen atom in the OH radicals and a H-atom bonded to an aromatic ring. They are located at ~1.1 to ~1.5 kcal $mol^{-1}$ below the products. With reaction energies around –6.0 to –6.4 kcal $mol^{-1}$, the removal of a hydrogen atom from naphthalene by a hydroxyl radical appears to be a rather strongly exothermic process.

Another pre-reactive complex with the OH radial on top of the ring has been found (Figure 4). The identified pre-reactive complexes can thus be referred to as *ipso*- and *ortho*- adducts (Figure 4). At the CBS-QB3 level of theory, the *ipso* and *ortho* intermediates have almost equal energies, with the *ipso* intermediate being more stable by 0.2 kcal $mol^{-1}$ only. These two pre-reactive complexes are connected by a very flat potential, so there is little chemical significance to this tiny energy difference except at very low temperatures.

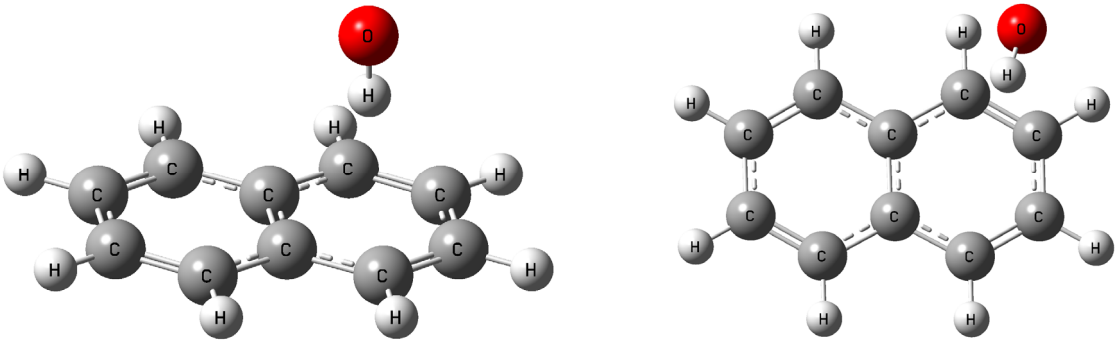

(a) The IM1-*ipso* structure (b) The IM1-*ortho* structure

**Figure 4.** Identified equilibrium structures for the pre-reactive intermediate IM1 (*ipso*- and *ortho*-), the loose complex between naphthalene and the OH radical.

### *3.2. Bond order analysis*

To follow the nature of the process, Wiberg bond indices have been computed according to a NBO analysis. There are several breaking/forming bond processes along the fragmentation process and the global nature of the reaction can be monitored by means of the so-called synchronicity ($S_y$):

$$S_y = 1 - \frac{\left[\sum_{i=1}^{n} \frac{\left|\delta B_i - \delta B_{av}\right|}{\delta B_{av}}\right]}{2n-2} \qquad (9)$$

In the above equation, $n$ is the number of bonds directly involved in the reaction and the relative variation of the bond index ($\delta B_i$) for a bond $i$ at the level of the transition state is estimated as follows:

$$\delta B_i = \frac{B_i^{TS} - B_i^{R}}{B_i^{P} - B_i^{R}} \qquad (10)$$

where the superscripts R, TS, and P refer to the reactants, transition states and products, respectively. The chemical reaction pathways **1** and **2** are characterized by a synchronicity value around ~0.81, which reveals a chemical process that is concerted, but not fully synchronic.

Hammond's postulate states that the structure of a transition state resembles that of the species nearest to it in free energy. This can be quantified in terms of a parameter *L*, defined as the ratio between the elongation of the C–H bond and the elongation of the H–O bond:

$$L = \frac{\delta r(\mathrm{C-H})}{\delta r(\mathrm{H-O})} \tag{13}$$

The values obtained for the parameter *L* for pathways **1** and **2** amount to 0.60 and 0.62, respectively, which confirms that the transition states are structurally closer to the reactants than to the products. These two reaction pathways being characterized by early transition states, they are expected to be exoergic.

### *3.3. Energetic and thermodynamic parameters*

A schematic potential energy diagram of the reaction pathways **1** and **2** is given in Figure 3. In line with the structural characteristics of the transition states, both reaction pathways **1** and **2** are exothermic ($\Delta H_r < 0$) and exoergic ($\Delta G_r < 0$) processes. Under thermodynamic control, i.e. at chemical equilibrium, the formation of 2-naphthyl should predominate. Spin contamination of the UHF electronic wave functions used at the start of all CBS-QB3 computations never exceeds 0.11 in the present study and can thus, for all practical purposes, be regarded as marginal. The obtained CBS-QB3 results may therefore safely be regarded as benchmark results.

### *3.4. Calculations of kinetic parameters*

Total and individual rate constants and the relative contribution from each pathway to the total rate constant at temperatures ranging from 636 to 873 K are listed and compared with available experimental values in Figure 5 and Table 7. As expected, $k_{-1}$ is considerably ($10^3$ times) larger than $k_2$, both on pathways **1** and **2**. We have assumed that the total rate constant ($k$) for the hydrogen abstraction process can be calculated as the sum of the individual rate constants for the two reaction pathways that are depicted in Figure 2:
$k_{total}=k_{overall}(\mathbf{1})+k_{overall}(\mathbf{2})$.

**Table 7.** Overall rate constants (in $cm^3$ $molecule^{-1}$ $s^{-1}$) and branching ratios (%) for the reported reaction channels at temperatures ranging from 636 to 873 K by means of TST theory ($P$ = 1.0 bar).

| $T$ (K) | Rate constant | | | | | | Branching ratio | | $k_{exp}$ [12-15] |
|---|---|---|---|---|---|---|---|---|---|
| | IM1→R $k_{-1}$ ($s^{-1}$) | IM1→P1 $k_{2a}$ ($s^{-1}$) | IM1→P2 $k_{2b}$ ($s^{-1}$) | R→P1 $k_{tot}(1)$ | R→P2 $k_{tot}(2)$ | $k_{tot}$ [$k(1)+k(2)$] | $R(1)$ | $R(2)$ | |
| 636 | $2.42\times10^{14}$ | $4.48\times10^{11}$ | $8.67\times10^{11}$ | $3.51\times10^{-12}$ | $6.78\times10^{-12}$ | $1.03\times10^{-11}$ | 34.05 | 65.95 | $(1.1\pm0.1)\times10^{-12}$ |
| 665 | $2.23\times10^{14}$ | $4.67\times10^{11}$ | $9.09\times10^{11}$ | $3.78\times10^{-12}$ | $7.36\times10^{-12}$ | $1.11\times10^{-11}$ | 33.93 | 66.07 | $(1.1\pm0.2)\times10^{-12}$ |
| 727 | $1.92\times10^{14}$ | $5.09\times10^{11}$ | $9.97\times10^{11}$ | $4.46\times10^{-12}$ | $8.74\times10^{-12}$ | $1.32\times10^{-11}$ | 33.79 | 66.21 | $(1.4\pm0.2)\times10^{-12}$ |
| 873 | $1.51\times10^{14}$ | $6.05\times10^{11}$ | $1.21\times10^{12}$ | $6.47\times10^{-12}$ | $1.29\times10^{-11}$ | $1.94\times10^{-11}$ | 33.40 | 66.60 | $(3.0\pm0.5)\times10^{-12}$ |

In line with energy barriers that do not differ by more than 0.24 kcal mol$^{-1}$ (see Figure 3), pathways **1** and **2** exhibit global kinetic rate constants of equal magnitude. Our computed rate constants are all in all in excellent agreement with experiment: they only differ by one order of magnitude. At the reported temperatures, the errors on the corresponding Gibb's free activation energies are therefore comprised between ~2.9 and 4.0 kcal mol$^{-1}$. These errors are quite acceptable, considering that the main contribution to Gibb's free reaction energies and activation energies are essentially entropic in origin. More elaborate treatments of statistical thermodynamical partition functions, taking dispersion forces, anharmonic effects and hindered rotations into account, are presumably needed for improving further the agreement between theory and experiment.

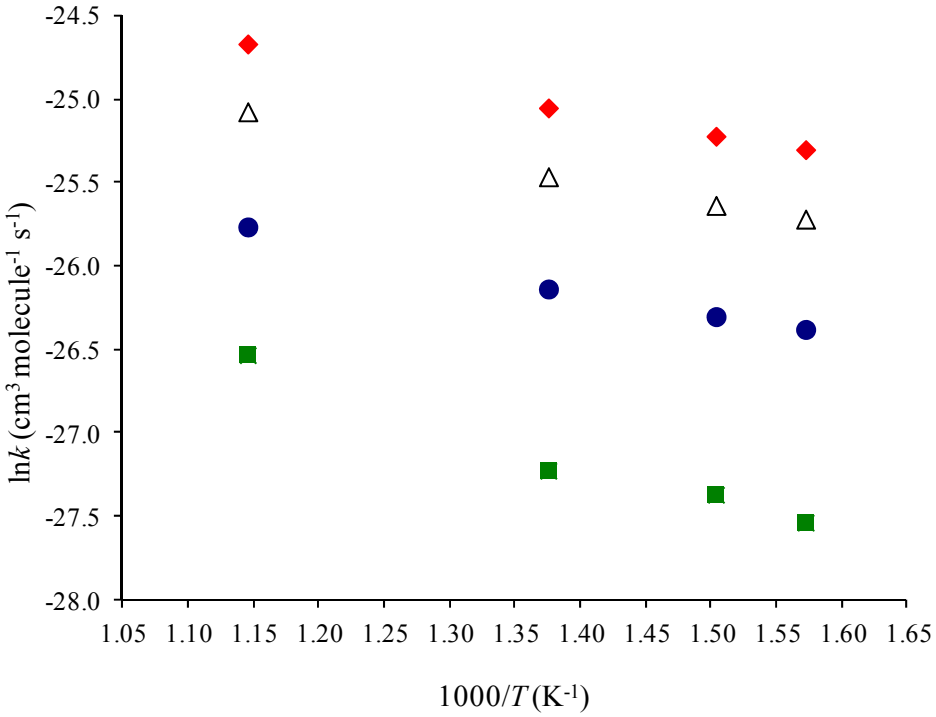


**Figure 5.** Arrhenius plot of our computed bimolecular rate constants versus experimental data. Legend: (●) theoretical rate constant for pathway 1; (△) theoretical rate constant for pathway 2; (◆) theoretical total rate constant for pathways 1 and 2; (■) experimental data.[12-15]

The rate constants for pathways **1** and **2** are almost equal, which indicates that there is no significant selectivity in site for the removal of a hydrogen atom. It can be seen from Table 7 that the rate constants increase gradually with increasing temperatures (Figure 6).

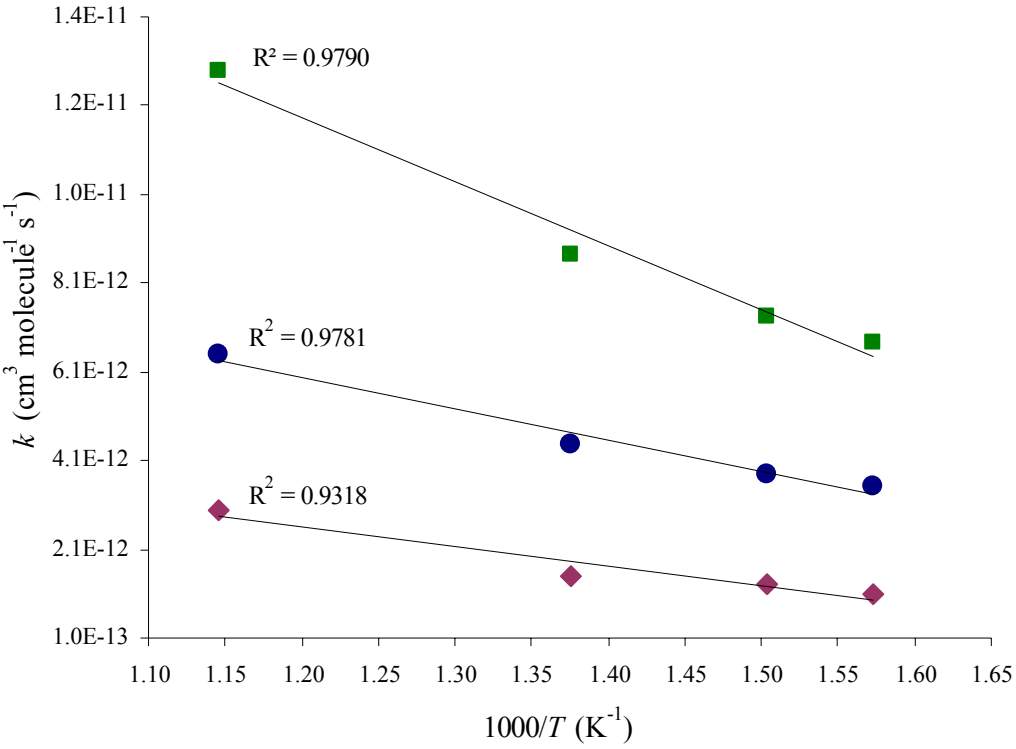


**Figure 6.** Plot of our computed bimolecular rate constants versus experimental data. Legend: (●) theoretical rate constant for pathway 1; (■) theoretical rate constant for pathway 2; (♦) experimental data.[12-15]

Branching ratios for the reaction pathways **1** and **2** are also reported in Table 7. These ratios were computed as follows:

$$R(1) = \frac{k_{R\rightarrow P1}}{k_{R\rightarrow P1} + k_{R\rightarrow P2}} \quad (16)$$

$$R(2) = \frac{k_{R\rightarrow P2}}{k_{R\rightarrow P1} + k_{R\rightarrow P2}} \quad (17)$$

These branching ratios only slightly vary with the temperature (Figure 7), which demonstrates that under the considered experimental conditions the removal of hydrogen atoms in naphthalene by a hydroxyl radical is essentially a non-selective process.

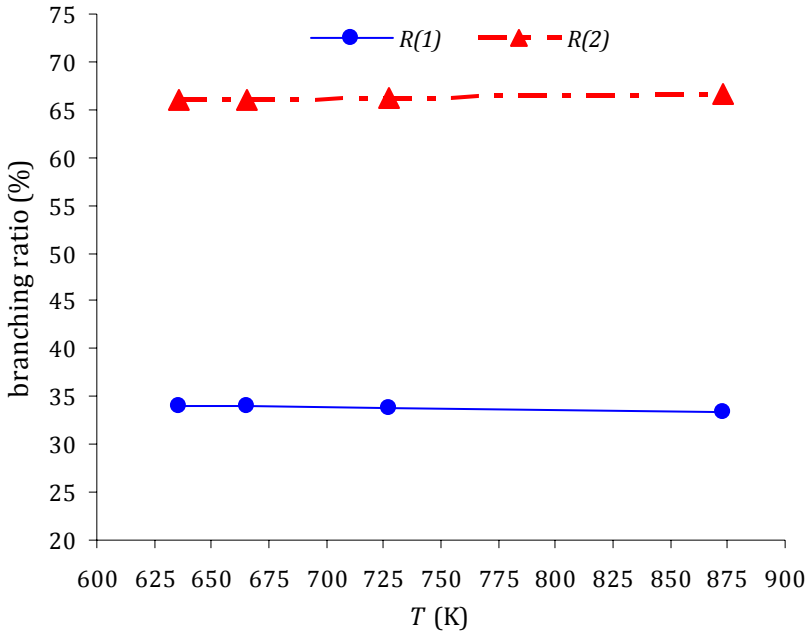


**Figure 7.** Evaluation of branching ratios in function of the temperature for pathways **1**–**2**.

## 4. CONCLUSIONS

Reaction mechanisms for the initial stages of naphthalene oxidation at high temperatures ($T \geq 600$ K) have been studied theoretically using the composite CBS-QB3 quantum chemical approach. Bimolecular kinetic rate constants were correspondingly estimated by means of transition state theory, on the grounds of partition functions calculated using the rigid rotor-harmonic oscillator approximation. The all-in-all rather excellent agreement with the available experimental kinetic rate constants confirms that a two-step reaction scheme prevails.

Analysis of the computed structures, bond orders, and free energy profiles demonstrate that the reaction steps involved in the removal of hydrogen atoms by OH radicals satisfy Hammond's principle. The energy profiles for removal of hydrogen atoms at the $C_1$ and $C_2$ positions are very similar, with differences in activation energies and reaction energies that do not exceed ~0.3 kcal $mol^{-1}$. Therefore, these reaction processes do not appear to exhibit a particularly pronounced site-selectivity: only a slight preference for a reaction at site $C_1$ and formation thereby of 1-naphthyl can be reported from the computed branching ratios.

## Reference

[1] A. Shiroudi, and M.S. Deleuze, J. Phys. Chem. A, *118* (**2014**) 3625.